


Tuning the Raman Resonance Behavior of Single-Walled Carbon Nanotubes via Covalent Functionalization

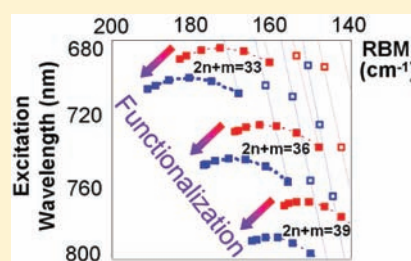
Jean-Yves Mevellec,[†] Céline Bergeret,[‡] Jack Cousseau,[‡] Jean-Pierre Buisson,[†] Christopher P. Ewels,[†] and Serge Lefrant^{*,†}

[†]University of Nantes, Institut des Matériaux Jean Rouxel, UMR CNRS 6502, 2 rue de la Houssinière, BP 32229, 44322 Nantes Cedex 03, France

[‡]University of Angers, Moltech Anjou, UMR CNRS 6200, 2 Boulevard Lavoisier, 49045 Angers Cedex 01, France

 Supporting Information

ABSTRACT: We present a systematic Raman study over a range of excitation energies of arc discharge single-walled carbon nanotubes (SWCNTs) covalently functionalized according to two processes, esterification and reductive alkylation. The SWCNTs are characterized by resonance Raman spectroscopy at each step of the functionalization process, showing changes in radial breathing mode frequencies and transition energies for both semiconducting and metallic tubes. Particular attention is given to a family of tubes clearly identified in the Kataura plot for which we continuously tune the excitation energy from 704 to 752 nm. This allows us to quantify the energy shift occurring in the spacing of the van Hove singularities. We demonstrate that, independently of the functionalization technique, the type of chain covalently bound to the tubes plays an important role, notably when oxygen atoms lie close to the tubes, inducing a larger shift in transition energy as compared to that of other carbonaceous chains. The study shows the complexity of interpreting Raman data and suggests many interpretations in the literature may need to be revisited.



INTRODUCTION

Since their first observation by high resolution transmission electron microscopy (HRTEM),^{1–3} single-walled carbon nanotubes (SWCNTs) have yielded a tremendous number of scientific studies⁴ in a large variety of domains and in particular applications. This interest is primarily due to their unique mechanical and electronic properties. SWCNTs have also attracted a great deal of attention in chemistry and many attempts have been made to functionalize them to tune their properties for specific applications. Many applications integrating SWCNTs require sample purification or modification by chemical treatments or else separation into either metallic or semiconducting tubes. The goal of this paper is not to review the main properties of the functionalized SWCNTs, since several feature papers^{5,6} have been devoted to this purpose, but to focus on the use of Raman spectroscopy as a tool to understand and quantify the role of specific carbon chains covalently attached to the SWCNT surfaces.

The chemistry of SWCNTs is now well developed.^{7–9} Chemical modification of SWCNTs is normally performed through organic functionalization, using both covalent or noncovalent strategies. Covalent techniques, recently reviewed,^{10,11} are numerous and can be divided into two primary groups: (a) amidation or esterification, following chemical oxidation of SWCNTs, and (b) direct functionalization of SWCNT sidewalls. We note here some key recent results from the literature. In the course of the amidation process leading to [60]fullerene-SWCNT hybrid materials bearing photoactive ferrocenyl or porphyrinyl

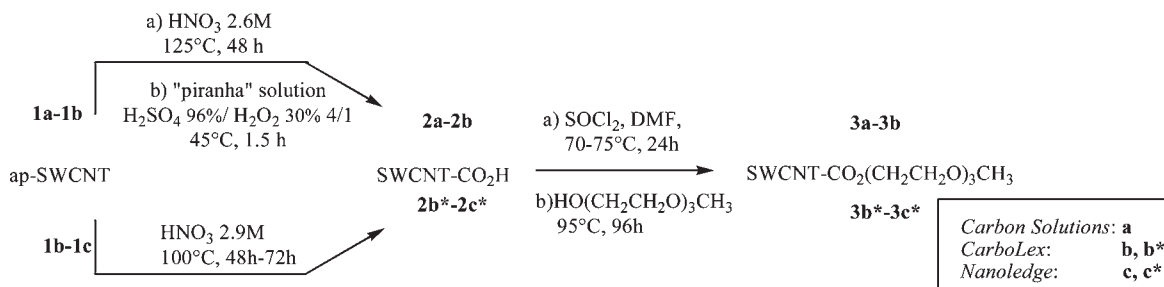
moieties,¹² the oxidation step was shown, from a Raman study, to destroy SWCNTs possessing diameters below 0.9 nm. In the field of direct functionalization, [2 + 2] cycloadditions of fluorinated olefins to SWCNTs were found to react preferentially with metallic tubes, this selective reactivity being attributed to the larger electron density near the Fermi level in such tubes,¹³ whereas 1,3-dipolar cycloaddition of pyridinium ylides appeared to be selective for metallic and large diameter semiconducting tubes.¹⁴ Click chemistry was also used for functionalizing SWCNTs with zinc porphyrins.¹⁵ Nucleophilic addition of lithium alkynylides R–C≡CLi takes place preferentially on smaller-diameter SWCNTs.¹⁶ The extent of alkylation of SWCNTs was shown to be well controlled from isolated SWCNT potassium salts, previously formed through chemical reduction of SWCNTs according to Pénicaud's procedure.¹⁷ Formylation of SWCNTs was performed, following reduction with BuLi.¹⁸ In addition, an elegant and efficient method was recently found to separate metallic and semiconducting SWCNTs because of the selective formation of molecular charge transfer salts characteristic of each family of tubes, after reaction of arc discharge SWCNTs with the potassium salt of coronene tetracarboxylic acid.¹⁹

Using combined physicochemical methods, we previously produced HiPCO carbon nanotubes initially purified by a nitric acid treatment and chemically treated to obtain SWCNT-ester derivatives. These derivatives were prepared to render the

Received: July 6, 2011

Published: September 17, 2011

Scheme 1. Preparation of SWCNT-Ester Derivatives



SWCNTs soluble in organic solvents for their use in organic solar cells, and were fully characterized via Raman, XPS, and FTIR spectroscopy.²⁰

Raman scattering is one of the most common techniques for characterizing carbon nanotubes. Spectra exhibit different behavior for semiconducting and metallic tubes. Additionally, radial breathing modes (RBMs) have frequencies inversely proportional to the tube diameter, providing an indication of the diameter distribution in a given sample. The RBM frequency is related to the tube diameter d via a relationship of the type ν (cm^{-1}) = A ($\text{cm}^{-1} \cdot \text{nm}$)/ d (nm) + B (cm^{-1}), in which A and B are parameters, the B term taking into account the environment interaction (see, for example, ref 21).

The so-called D band is commonly assigned to defects in carbon structures.²² Normally forbidden in the first-order Raman spectrum, it has been shown recently to originate from a second order Raman process.²³ For a long time the D/G intensity ratio was used to evaluate the sample defect concentration (and hence functionalization). However D. Abdula et al.²⁴ demonstrate that this should be done with care, and in any case, one should take into account the line shape of the "G" band.

These features are of course criteria to follow the modifications induced by different chemical treatments used to functionalize nanotubes. In a previous study of HiPCO tube functionalization, we showed that, despite a drastic change in the G band profile of metallic tubes, the RBM intensities decreased during functionalization, coupled with an upshift of their frequencies.²⁰

Even if a clear description of functionalized tubes requires more detailed simulation, the presence of impurities like oxygen has been shown to induce a modification in the conductance of metallic tubes.²⁵ We may invoke similar arguments in our case. For semiconducting tubes, we observe smaller effects on Raman spectra that we interpreted as a signature of a weaker efficiency of the functionalization. The same results were also reported in the literature. For example, Liu et al. have chemically grafted methoxyphenol functions on SWCNTs and observed a preferential reactivity for metallic and smaller diameter semiconducting tubes.²⁶

In this paper, we report on studies carried out on arc discharge functionalized tubes. We have investigated in detail the modification of RBM frequencies. In particular, we have followed the resonance conditions using a Ti-sapphire laser, changing the excitation wavelength in steps of 4 nm. We demonstrate for the first time that the nature of the group which is covalently bonded to the carbon nanotubes is of primary importance with regards to both Raman peak frequency and intensity criteria associated to functionalized tubes. These results are of primary importance for both chemists and physicists working with functionalized carbon nanotubes, showing the necessity for critical analysis of Raman

spectra based on choice of laser excitation wavelength, as well as the precise nature of the chosen functional groups.

RESULTS AND DISCUSSION

Functionalization Processes. We use arc-discharge SWCNTs (referred to as as-produced ap-SWCNTs hereafter) from three sources, namely Carbon Solutions, CarboLex and Nanoledge. These were covalently functionalized using two different processes: (i) esterification of SWCNTs following the formation of carboxylic acid derivatives⁹ SWCNT-CO₂H and (ii) reductive alkylation through Pénicaud's procedure,^{27,28} leading to SWCNT-R derivatives. SWCNT-ester derivatives were obtained via standard methods (Scheme 1). In the first process, the ap-SWCNTs **1a–1b** were first purified and oxidized in two steps by treatment with boiling 2.6 M aq. nitric acid, then with H₂SO₄/H₂O₂ "piranha" mixture,^{29–31} resulting in SWCNT-CO₂H derivatives **2a–2b**. In a second method, oxidation of ap-SWCNTs **1b–1c** was performed using more concentrated 2.9 M HNO₃ to enhance the concentration of carboxylic acid sites³² in corresponding SWCNT-CO₂H derivatives **2b*–2c***, confirmed via thermogravimetric analysis (TGA) provided for **2b** and **2b*** samples (see Figure 1 in Supporting Information). After conversion of the carboxylic acid sites into acyl chloride groups,²⁹ reacting with alcohol HO(CH₂CH₂O)₃CH₃ resulted in the SWCNT-ester derivatives **3a, 3b, 3b***, and **3c***.

Chemical reduction of ap-SWCNTs, performed in a glovebox from the reaction of Na⁺/naphthalene complex in tetrahydrofuran (THF), showed that CarboLex SWCNTs are very weakly reduced (see experimental description below). As a consequence, the reaction of halo derivatives $n\text{C}_{12}\text{H}_{25}\text{I}$ and $\text{BrCH}_2\text{CO}_2\text{CH}_2\text{CH}_2\text{OCH}_3$ was studied only with reduced SWCNTs **4a** and **4c** using Carbon Solutions and Nanoledge tubes, respectively (Scheme 2). These reactions, carried out in dimethyl sulfoxide (DMSO) at room temperature, led to the expected SWCNT- $n\text{C}_{12}\text{H}_{25}$ **5a** and **5c**, and SWCNT-CH₂-CO₂CH₂CH₂OCH₃ **6c** samples.

TGA. TGA in an argon atmosphere ($\Delta T = 10^\circ\text{C} \cdot \text{min}^{-1}$) was performed for SWCNT derivatives issued from the different steps of the functionalization processes presented above, in order to evaluate their respective efficiency. Samples **2a–2b** display a clear weight loss in the 180–350 °C interval (Figure 1, Supporting Information), ~6–7%, probably due to a CO₂ release from carboxylic acid sites.³³ A more important ~20% weight loss was observed from samples **3a–3b**, which is consistent with the expected pyrolysis of the ester groups, as already observed from comparable SWCNT derivatives.³⁴ The equivalent weight losses issued from samples **2b*** and **2c*** are ~10–12%, and ~26% and 30% for samples **3b*** and **3c*** respectively. From these latter results, the degrees of functionalization can be estimated as one

Scheme 2. Preparation of SWCNT-R Derivatives

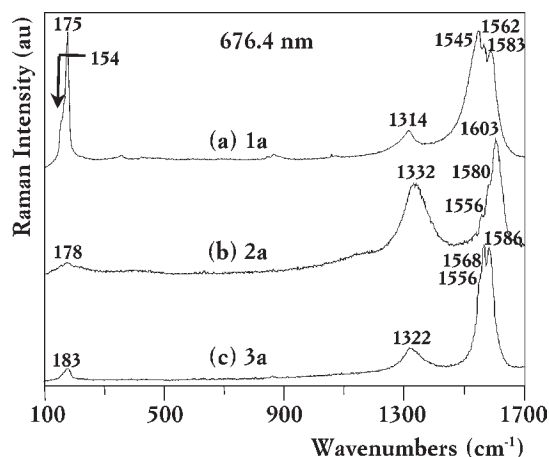
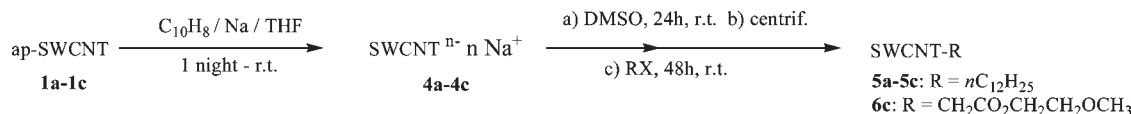


Figure 1. Raman spectra of Carbon Solutions single-walled nanotubes with an excitation wavelength of 676.4 nm, $T = 300\text{K}$. (a) Pristine: 1a. (b) Washed with HNO_3 and oxidized: 2a. (c) Functionalized: 3a.

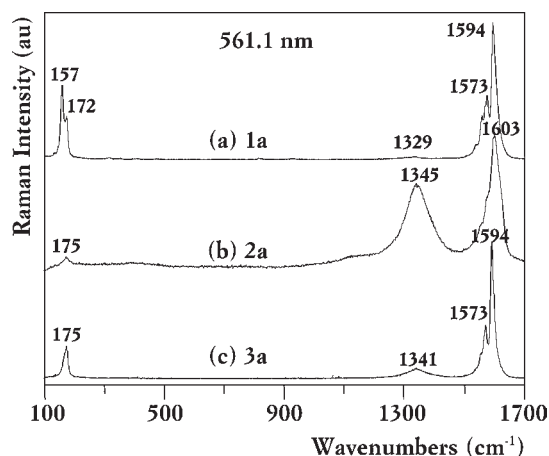


Figure 2. Raman spectra of Carbon Solutions single-walled nanotubes with an excitation wavelength of 561.1 nm, $T = 300\text{K}$. (a) Pristine: 1a. (b) Washed with HNO_3 and oxidized: 2a. (c) Functionalized: 3a.

ester group for every ~ 68 (3a), 60 (3b), 45 (3b*) and 45 (3c*) nanotube carbons, respectively. The TGA for samples 5a, 5c, and 6c (Figure 2, Supporting Information), derived from the reduction-alkylation procedure, showed a weight loss in the 150–450 °C interval, ~ 19 –20%, associated with the pyrolysis of the alkyl group. The corresponding degrees of alkylation can be evaluated as one $\text{R} = \text{C}_{12}\text{H}_{25}$ group for every ~ 59 (5a) and 57 (5c) nanotube carbons and one $\text{R} = \text{CH}_2\text{CO}_2\text{CH}_2\text{CH}_2\text{OCH}_3$ group for every ~ 30 (6c) nanotube carbons.

Raman Scattering. For arc discharge tubes, one excitation wavelength, that is, $\lambda_{\text{exc.}} = 676.4\text{ nm}$, is only in resonance with transitions of metallic tubes whereas semiconducting tubes are

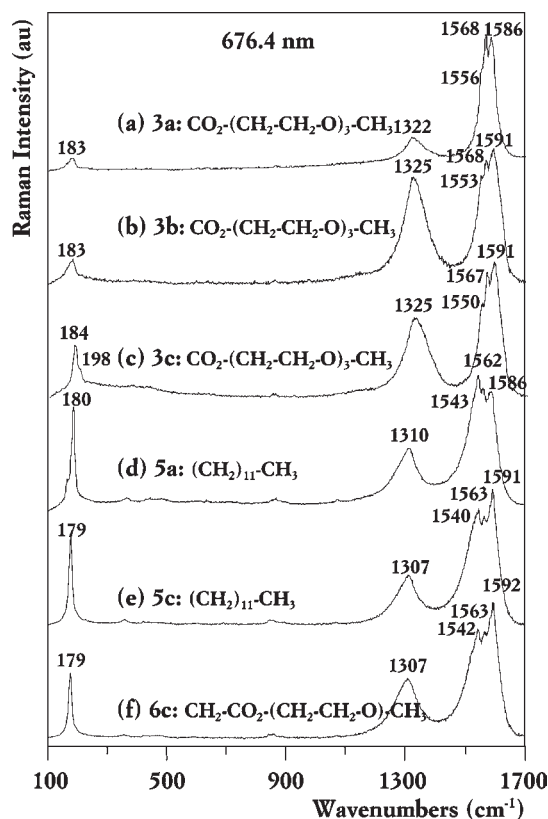


Figure 3. Raman spectra of functionalized SWCNTs-R. $\lambda_{\text{exc.}} = 676.4\text{ nm}$, $T = 300\text{ K}$. (a, b, and c) $\text{R} = \text{CO}_2-(\text{CH}_2-\text{CH}_2-\text{O})_3-\text{CH}_3$. (d and e) $\text{R} = (\text{CH}_2)_{11}-\text{CH}_3$. (f) $\text{R} = \text{CH}_2-\text{CO}_2-(\text{CH}_2-\text{CH}_2-\text{O})-\text{CH}_3$. (a and d) Carbon Solutions SWCNTs; (b) CarboLex SWCNTs; (c, e, and f) Nanoledge SWCNTs.

usually observed either at a longer (1064 nm) or at a smaller wavelengths (514.5 nm or other). In Figures 1 and 2, we present data from Carbon solutions SWCNTs, at each step of the functionalization process via nitric acid purification (Scheme 1), since samples from other sources provide similar results. Figure 1 shows the Raman spectra at $\lambda_{\text{exc.}} = 676.4\text{ nm}$, that is, for metallic tubes. Curve a exhibits the usual features of metallic tubes with RBM frequencies at 154 (shoulder) and 175 cm^{-1} , a G band with several components, especially in the low energy side and a clear asymmetric profile. The D band is reasonably weak. After purification with nitric acid and further oxidation (curve b), we observe several modifications: (i) a strong decrease of the radial breathing mode intensity, (ii) an intensity increase of the D band, and (iii) a strong decrease of the low frequency components of the G band. This is similar to previous observations of HiPCO tubes.²⁰ The primary RBM frequency is slightly up-shifted, from 175 to 178 cm^{-1} . Curve c shows the Raman spectrum after covalent functionalization with a $-\text{CO}_2-(\text{CH}_2\text{CH}_2\text{O})_3-\text{CH}_3$ group (scheme.1). The RBM frequency is further up-shifted to

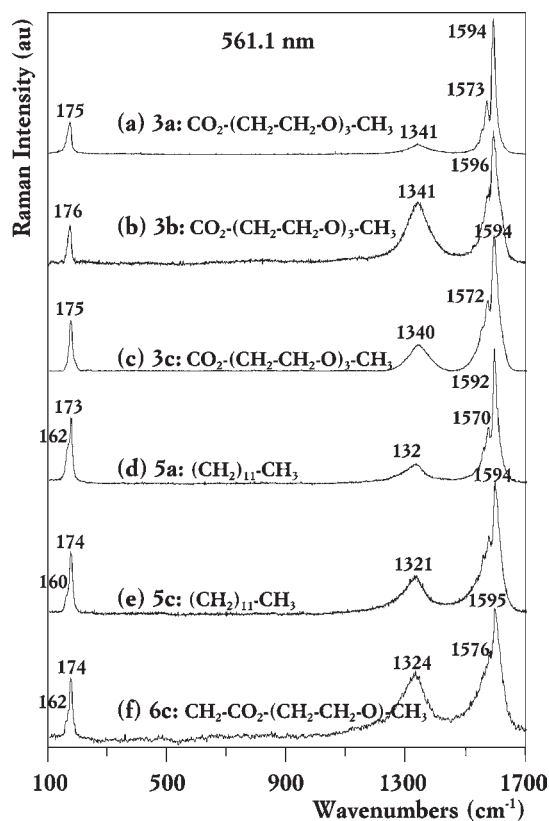


Figure 4. Raman spectra of functionalized SWCNTs-R. $\lambda_{\text{exc.}} = 561.1$ nm, $T = 300$ K. (a, b, and c) $R = \text{CO}_2-(\text{CH}_2-\text{CH}_2-\text{O})_3-\text{CH}_3$, (d and e) $R = (\text{CH}_2)_{11}-\text{CH}_3$, (f) $R = \text{CH}_2-\text{CO}_2-(\text{CH}_2-\text{CH}_2-\text{O})-\text{CH}_3$, (a and d) Carbon Solutions SWCNTs; (b) CarboLex SWCNTs; (c, e, and f) Nanoledge SWCNTs.

183 cm^{-1} , the D band has considerably decreased and the low frequency component of the G band is partially restored.

For studying semiconducting tubes, we have chosen $\lambda_{\text{exc.}} = 561.1$ nm (Figure.2), and we see similar modifications, that is, an increase of the D band after purification, a decrease of the RBM intensity and less structured features in the G band. After functionalization, one observes only one RBM band peaked at $\sim 175\text{ cm}^{-1}$, the D band is weak and the G band is restored. The oxidative step looks less efficient than for metallic tubes. The RBM mode at 175 cm^{-1} corresponds to that at 172 cm^{-1} in curve (a); its relative shift is discussed below.

Figures 3 and 4 show Raman spectra of SWCNTs issued from the three different sources and functionalized with different groups, using excitations at 676.4 and 561.1 nm, respectively. Behavior similar to that described above is globally observed.

As examples, curves a, b, and c of Figures 3 and 4 represent spectra for the same functionalization procedure using SWCNTs from different origins. By comparison with pristine samples (see curves a of Figures 1 and 2), the only major difference is a weaker D band for Carbon Solutions samples which was already the case before functionalization. This may just indicate a better purified pristine sample. We also observe a slight increase of the RBM frequencies and a decrease of their intensity. In a second series (curves d, e, and f), we show Raman spectra of samples functionalized according to Scheme 2. These results resemble those described in curves a, b, and c, although somewhat less pronounced. The RBM frequency shifts are reduced from 175 to

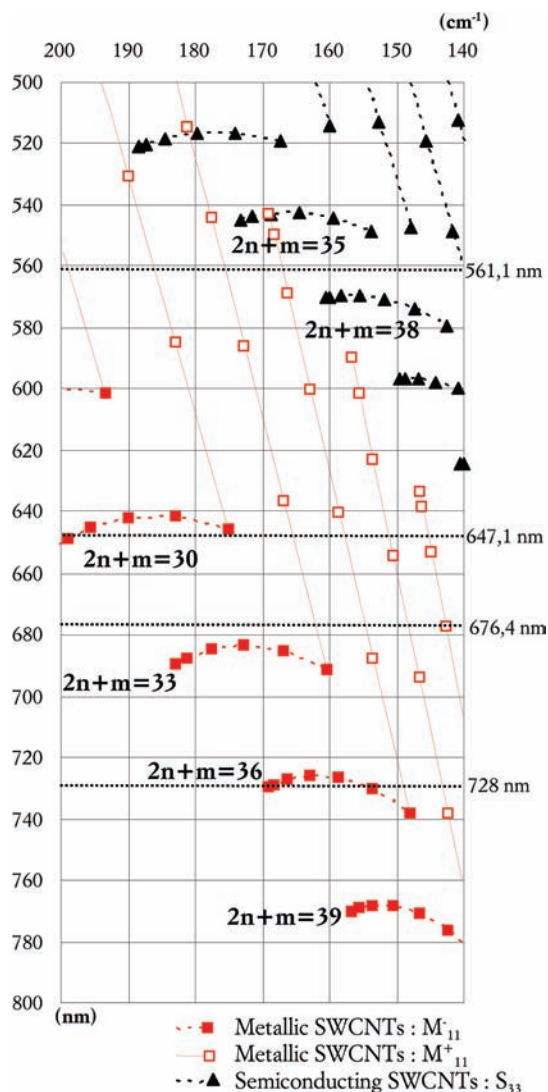


Figure 5. Experimental Kataura plot: SWCNTs gap energies fitted on experimental data in the bundle form. Red squares indicate metallic SWCNTs and black triangles semiconducting ones. Open squares correspond to high energy transitions. Nanotubes of the same family are connected by diagonal straight lines.

$179-180\text{ cm}^{-1}$ instead of $183-4\text{ cm}^{-1}$ (Figure.3). Thus these results show that Raman spectra appear to be similar independent of tube preparation method. On the contrary, the nature of the functional group attached to the tubes plays a larger role in the frequency shifts of the RBMs, as discussed below.

Figure.5 shows a partial and detailed region of the Kataura plot³⁵ adapted for studying “arc discharge” nanotubes with RBM frequencies in the range $140-200\text{ cm}^{-1}$, that is, for diameters between 1.19 and 1.75 nm. The different frequencies vs their transition energies were recalculated from both experimental data and literature. Notably the energy transitions S_{33} and M_{11} shown in Figure 5 are calculated from empiric formulas,³⁶ given in the Supporting Information. For the relationship $\nu\text{ (cm}^{-1}\text{)} = A\text{ (cm}^{-1}\cdot\text{nm)}/d\text{ (nm)} + B\text{ (cm}^{-1}\text{)}$, we have chosen $A = 223.5\text{ (cm}^{-1}\cdot\text{nm)}$ and $B = 12.5\text{ (cm}^{-1}\text{)}$, which provide good results²¹ for tubes with diameters d larger than 0.7 nm.

We have collected data in families defined with $2n + m = N$ for tubes with Hamada index (m,n) , n and m being the integers

which define the tube chirality, tubes being metallic whenever N is a multiple of 3 and semiconducting otherwise. To understand the RBM intensity and its variation as a function of the laser wavelength, it is necessary to identify the tubes present in our samples.

Figure 5 indicates tubes whose transition energies are close to the excitation laser energy. The excitation $\lambda_{\text{exc.}} = 676.4$ nm clearly shows that the nearest tubes are metallic belonging to the $2n + m = 33$ family, whereas $\lambda_{\text{exc.}} = 561.1$ nm reveals mainly semiconducting tubes involving two branches defined by $2n + m = 35$ and 38 , respectively. The intensity of the Raman peaks is monitored by an equation of the following type:³⁷

$$I(E_L) = \int \left| \frac{Mg(E)}{(E_L - E - i\Gamma_r)(E_L \pm E_{\text{ph}} - E - i\Gamma_r)} \right|^2 dE \quad (1)$$

where E_{ph} is the phonon energy, E_L the energy of the excitation light, M the moment of the transition, and $g(E)$ the joint density of states. Signs + or - stand for the Stokes and anti-Stokes intensities, respectively. This equation shows in particular that the proximity of E_L and E greatly enhances the intensity of the Raman response and that an off-resonance excitation will not give a Raman signal. Any modification of the density of states and of the Van Hove singularities and consequently of the electronic transition values will therefore affect the intensity of the whole Raman spectrum, but not a decrease of the RBM intensity with respect to the other modes.

Therefore, one has to analyze RBM data in greater details. For example, the RBM band at 175 cm^{-1} shown in Figure 1, curve a ($\lambda_{\text{exc.}} = 676.4$ nm) corresponds to the $2n + m = 33$ branch of metallic tubes and is composed of 6 components with close frequencies which possess approximately the same transition energies. Consequently, one observes only one band. This situation occurs whenever the branch $2n + m$ is horizontal, that is corresponding to tubes with the same energy transition but different RBM frequencies. As a consequence, several tubes belonging to the same branch contribute to one Raman band. Another example is shown in Figure 5. The excitation at 561.1 nm is situated between the 2 branches $2n + m = 35$ and $2n + m = 38$ of semiconducting tubes (S_{33}) and one then obtains 2 Raman peaks at 157 et 172 cm^{-1} , respectively. This is better illustrated in Figure 6 in which we have performed the decomposition of the band corresponding to the $2n + m = 36$ branch of metallic tubes, observable with the 728 nm excitation. In Table 1, we have collected the frequency and the full width at half-maximum (fwhm) of each component derived from the decomposition. We can observe that all expected tubes provide their own contribution. The maximum intensity contribution is provided by the tube whose transition energy is the closest to the excitation. The widths at half-maximum have been taken between 4.8 and 7.9 cm^{-1} , similarly to those observed by Meyer et al³⁸ on Raman spectra of isolated and suspended nanotubes. The difference between the fwhm of each individual component can be related to the presence of small bundles (see Table 1). Notice that in the case of metallic tubes, formula (2) (see Supporting Information) leads to two different values (except for armchair tubes ($n = m$)) for the absorption energy E_{11}^{\pm} (M) depending on the + or - sign, and those corresponding to the highest values (open squares, Figure 5) are also observed experimentally. This is the case, for example, for the shoulder seen at

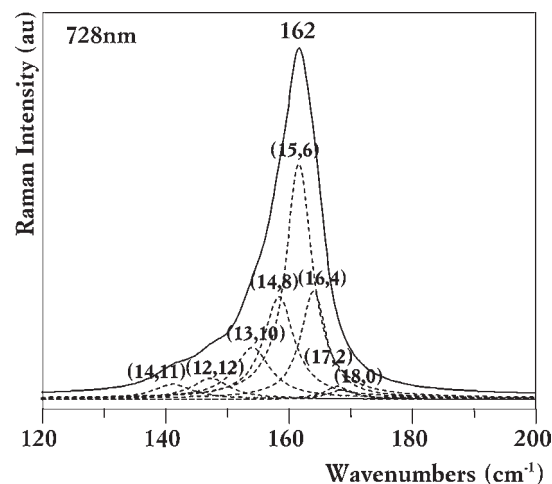


Figure 6. Raman spectra decomposition of the RBM band observed for Pristine Carbon Solutions (1a). The excitation wavelength is 728 nm , $T = 300 \text{ K}$.

Table 1. Decomposition of the RBM Raman Band of Pristine Carbon Solutions SWCNTs (1a) for an Excitation of 728 nm^a

| $2n + m$ | (n,m) | E_r (nm) | fwhm (cm^{-1}) | frequency (cm^{-1}) |
|----------|---------|------------|---------------------------|--------------------------------|
| 36 | (18,0) | 728 | 4.93 | 169 |
| 36 | (17,2) | 727 | 4.80 | 168 |
| 36 | (16,4) | 725 | 4.98 | 166 |
| 36 | (15,6) | 724 | 5.12 | 163 |
| 36 | (14,8) | 725 | 6.00 | 159 |
| 36 | (13,10) | 728 | 7.02 | 153 |
| 36 | (12,12) | 736 | 7.88 | 148 |
| 39 | (14,11) | 738 | 7.88 | 142 |

^a fwhm: full width at half maximum.

154 cm^{-1} for $\lambda_{\text{exc.}} = 676.4 \text{ nm}$ (Figure 1a), that we assign to the (13,10) tube of the $2n + m = 36$ branch. On the other hand, the lowest value in energy corresponding to this tube participates to the spectrum recorded for $\lambda_{\text{exc.}} = 728 \text{ nm}$ (see Table 1).

Besides a clear identification of the tubes present in our samples, the nature of the group covalently bounded to the SWCNTs seems to play a significant role, independently of the tube source and the method used to achieve the functionalization. As an example, in all cases when a $-\text{CO}_2-(\text{CH}_2\text{CH}_2\text{O})_3-\text{CH}_3$ group (for example sample 3a) is attached to the tubes, the RBM frequency seems to be up-shifted to a larger extent than with a group without oxygen (samples 5a–5c). In order to check this point, we have carried out careful experiments with different laser excitation energies issued from a Ti-sapphire laser. We tuned the excitation from 704 to 752 nm in steps of 4 nm on the same sample position. The spectra are shown on Figure 7 for three different samples in the Carbon Solutions series: pristine, functionalized with $-(\text{CH}_2)_{11}-\text{CH}_3$ groups and functionalized with $-\text{CO}_2-(\text{CH}_2\text{CH}_2\text{O})_3-\text{CH}_3$ groups. Fortunately, the branch corresponding to the metallic family characterized by $2n + m = 36$ lies between 720 and 740 nm , in a range suitable for using a continuous Ti-sapphire laser.

The tubes we are observing with these excitations are well identified by both their frequencies and energy transitions (see Table 1). The intensity of the most intense mode at $\sim 162 \text{ cm}^{-1}$

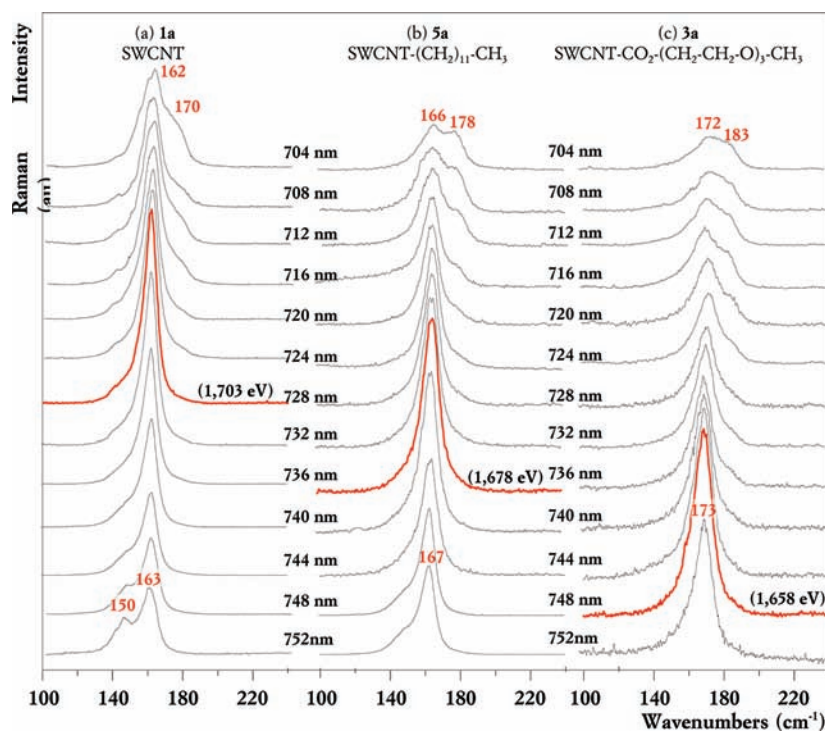


Figure 7. Raman spectra of Carbon Solutions nanotubes with an excitation wavelength from 704 to 752 nm by step of 4 nm, $T = 300$ K. Intensities have been normalized to the most intense response. (a) Sample 1a, (b) sample 5a, and (c) sample 3a.

for the pristine material has been measured with great care for all excitation lines and the maximum is observed for $\lambda_{\text{exc.}} = 728$ nm, in agreement with what is shown Figure 5. Notice that if the excitation is below or above this value, other modes at 170 cm^{-1} (for $\lambda_{\text{exc.}} = 704$ nm) and 150 cm^{-1} ($\lambda_{\text{exc.}} = 752$ nm) are observed because one catches the resonance from tubes corresponding to horizontal neighboring branches.

The precise determination of the maximum resonance can be made using eq 1, provided the number of tube families involved is small and their nature well-defined, here metallic ones. In such a case, one can then evaluate the type of modification of the electronic transition induced by the functionalization. This is an important point since the intensity of the RBMs is always seen as decreasing after a chemical treatment. This may have several origins, one of them being the remoteness from resonance conditions.

To elucidate this point, we have carried out identical Raman investigations for the same branch of tubes with two different functional groups covalently bounded to them. In the first case, that is, for groups of the type $-(\text{CH}_2)_{11}-\text{CH}_3$, the maximum intensity is clearly shifted to 736 nm. In the second case when groups of the type $-\text{CO}_2-(\text{CH}_2\text{CH}_2\text{O})_3-\text{CH}_3$ are attached to the tubes, the resonance is further shifted to 748 nm. These results illustrate why any comment on the intensity of RBM is a difficult task which has to be taken with great care. In addition, we note that Raman data obtained on sample 6c are similar to those of samples 5a and 5c, despite the fact that the $(-\text{CH}_2-\text{CO}_2-(\text{CH}_2\text{CH}_2\text{O})-\text{CH}_3)$ group contains a CO_2 . But in this case, the oxygen atom is not adjacent to the tube. Therefore, this demonstrates clearly that the vicinity of oxygen atoms induces a large modification of the electronic levels and energy transitions. In Figure 7 one observes that the RBM is globally shifted in the same manner once functionalization is achieved, that is, this shift applies to all its components.

We have therefore built the modified Kataura plot portion shown in Figure 8 by applying the maximum observed shift induced by the functionalization by the $(-\text{CO}_2-(\text{CH}_2\text{CH}_2\text{O})_3-\text{CH}_3)$ group to all tubes. We have translated the transition energy from 1.703 (728 nm) to 1.660 eV (747 nm) and the frequency of the main RBM band from 162 to 173 cm^{-1} . In this way, one can better explain what is observed after functionalization.

At $\lambda_{\text{exc.}} = 561.1$ nm, as already mentioned, the excitation energy lies between two branches (Figure.5) and as a consequence, the RBM band is composed of mainly two components at 157 and 172 cm^{-1} , respectively (Figure.2a). The functionalization induces a decrease of the resonance energy and then, the $2n + m = 38$ branch, which provided the most intense band in the initial spectrum (157 cm^{-1}), is now away from the excitation (Figure 8). On the other hand, this band appears, after functionalization, only as a shoulder shifted to $160-162 \text{ cm}^{-1}$ and it even disappears (Figure.4). On the contrary, for the same reasons, the resonance increases for the $2n + m = 35$ branch (Figure 8) and the experimental RBM frequencies are shifted from 172 to 175 cm^{-1} with an intensity increase. The shift of the RBM frequencies thus provides a better indication of the functionalization than that given by intensity decrease. Keeping this in mind, it seems that all the observed effects are weaker in the case of semiconducting tubes, the upshift of the RBM frequencies being only 3 cm^{-1} . This was indicated in our previous studies devoted to the functionalization of HiPCO tubes and therefore is somewhat confirmed in the case of functionalized “arc discharge” tubes.

It may happen that, for a given excitation wavelength, we do not observe the same tubes before and after esterification. As an example, for $\lambda_{\text{exc.}} = 676.4$ nm, the RBM band is observed at 175 cm^{-1} for pristine tubes (Figure 1a), corresponding to the resonance with the $2n + m = 33$ branch family. This band is

up-shifted to 183 cm^{-1} after functionalization (Figure 1c). On the basis of the diagram shown in Figure 8, we also expect to

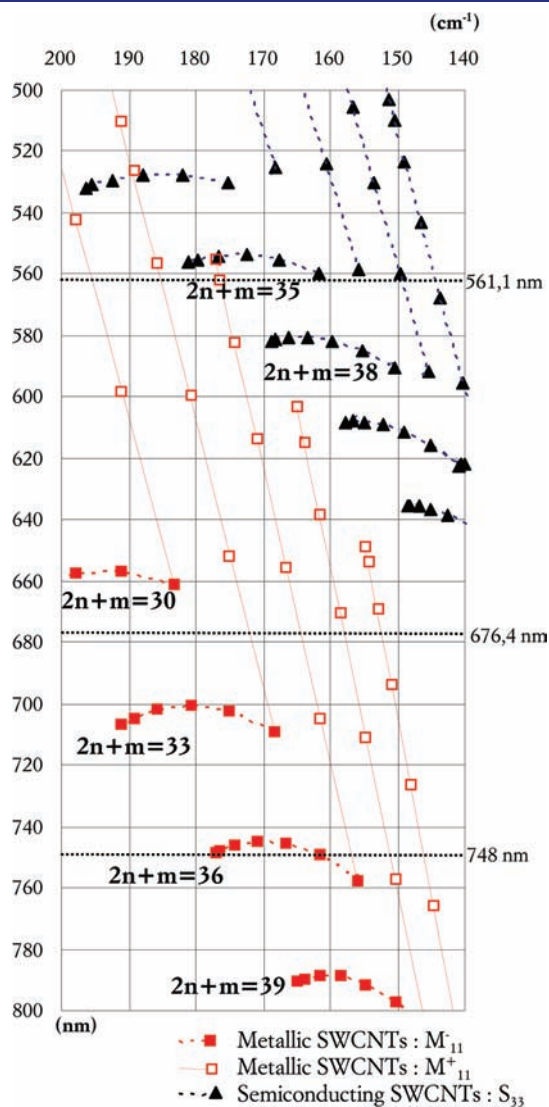


Figure 8. Experimental Kataura Plot: SWCNT- $\text{CO}_2-(\text{CH}_2-\text{CO}_2-\text{O})_3-\text{CH}_3$ gap energies in the bundle form. Red squares indicate metallic SWCNTs and black triangles semiconducting ones. Open squares correspond to high energy transitions. Nanotubes of the same family are connected by diagonal straight lines.

observe the RBM band of the $2n + m = 30$ branch with a rather significant intensity. Before functionalization, we can see that we are clearly in resonance with the transitions of this branch for an excitation at 647.1 nm (indicated by a horizontal line on Figure 5). But, when one compares the RBM for arc discharge and HiPCO tubes at this excitation, (see Supporting Information, Figure 3), the intense mode at 194 cm^{-1} for HiPCO tubes is not present for arc discharge tubes, demonstrating that tubes corresponding to these diameters are not present in pristine arc discharge SWNTs. Therefore, one can deduce from this analysis that the modified Kataura plot is rather valuable to explain the observed Raman data after functionalization.

Results shown in Figure 7 for Carbon Solutions samples have also been obtained with tubes issued from different sources and functionalized with different chains. We have collected in Table 2 the data, in particular the maximum intensity of the RBMs recorded in the range $704-752\text{ nm}$, that is, for the $2n + m = 36$ tube family.

For samples issued from different sources, we observe the same results in frequency and resonance energy after the same chemical treatment. In particular, we confirm that the resonance shift is larger when the chain substitution includes an oxygen atom close to the tubes. For those tubes, whose Raman spectra are presented in Figure 7, we obtain a shift of 0.021 eV for samples 5a, a shift which is doubled to 0.043 eV for samples 3a. Notice that a very strong oxidation can lead to a further shift in the resonance energy (Table 2, sample 3c*) for which a value of 0.061 eV was obtained. This effect has been recently confirmed by Müller et al. in propylene-functionalized SWNTs.³⁹ Therefore, we interpret the shift in the resonance energy changes as due to two different effects, one is due to the functionalization itself, whereas a second effect originates from the presence of an electron acceptor in the chain (here an oxygen atom) in the close vicinity of the tubes, acting as a dopant.

In order to corroborate this point, we have carried out DFT calculations on (6,6) nanotubes as an example to evaluate first the spacing between the first van Hove singularities and then the radial breathing mode frequency in various charge states. In this example, the resonance energy is calculated at 2.424 eV and the RBM frequency at 275 cm^{-1} . From these very preliminary calculations, it seems that upon ionization, that is, removing or adding electrons from or to the tubes, the resonance energy slightly shifts downward ($\sim 0.02\text{ eV}$) as observed in our experiments for the case of electron loss. On the other hand, the effect of ionization is not sufficient to explain the upshift in the RBM frequencies, a more complex calculation including the covalently bounded chains being certainly necessary.

Table 2. Experimental Frequencies and Resonance Energies E_r for the Main RBM Raman Band in the Frequency Range $704-752\text{ nm}$

| powders | name ^a | grafted group | E_r (nm) | E_r (eV) | ν (cm^{-1}) |
|--|-------------------|--|------------|------------|----------------------------|
| Pristine SWCNTs | 1a | | 728 | 1.703 | 163 |
| | 1b | | 726 | 1.708 | 161 |
| | 1c | | 726 | 1.708 | 163 |
| SWCNTs functionalized Via the polyanions SWCNT ⁿ⁻ | 5a | $(\text{CH}_2)_{11}-\text{CH}_3$ | 737 | 1.682 | 167 |
| | 5c | $(\text{CH}_2)_{11}-\text{CH}_3$ | 737 | 1.682 | 167 |
| | 6c | $\text{CH}_2-\text{CO}_2-(\text{CH}_2\text{CH}_2\text{O})-\text{CH}_3$ | 738 | 1.680 | 167 |
| | 3a | $\text{CO}_2-(\text{CH}_2\text{CH}_2\text{O})_3-\text{CH}_3$ | 747 | 1.660 | 171 |
| SWCNTs functionalized By oxidative way | 3b | $\text{CO}_2-(\text{CH}_2\text{CH}_2\text{O})_3-\text{CH}_3$ | 747 | 1.660 | 171 |
| | 3b ^b | $\text{CO}_2-(\text{CH}_2\text{CH}_2\text{O})_3-\text{CH}_3$ | 750 | 1.653 | 173 |
| | 3c ^b | $\text{CO}_2-(\text{CH}_2\text{CH}_2\text{O})_3-\text{CH}_3$ | 753 | 1.647 | 173 |
| | 3c* | $\text{CO}_2-(\text{CH}_2\text{CH}_2\text{O})_3-\text{CH}_3$ | 753 | 1.647 | 173 |

^a a: Carbon Solutions b: CarboLex c: Nanoledge. ^b Stronger oxidative process (see text).

CONCLUSION

In conclusion, we have used resonance Raman spectroscopy to analyze in detail covalently functionalized arc discharge SWCNTs at each step of the functionalization. By using different excitation wavelengths, we have followed the change in behavior of both semiconducting and metallic tubes.

We find a down shift of RBM frequencies after functionalization of typically $3\text{--}4\text{ cm}^{-1}$ for samples such as **3a** and of $7\text{--}8\text{ cm}^{-1}$ when oxygen lies close to the tubes (sample **5a**). Using a refined Kataura plot and selecting a particular tube family, we have shown that the nanotube resonance energy decreases upon functionalization, by an amount which is clearly dependent upon the type of group that is attached to the SWCNTs, but is independent of the method of functionalization and the nanotube origin.

A continuous change in the excitation energy has permitted us to quantify this modification which is found to be 0.021 eV for carbonaceous chains, reaching 0.043 eV when an oxygen atom lies in the close vicinity of the tubes. This is interpreted as a result of electron transfer as may occur in doped systems.

These results have profound implications for interpretation of resonant Raman data in the literature for nanotube functionalization. Notably a decrease in peak intensity does not necessarily imply successful functionalization of a given tube type: indeed the downshift in resonance energy associated with charge transfer after functionalization could bring the resonance energy of some tubes closer to the laser excitation energy and actually increase RBM peak intensity. Thus, we suggest that RBM peak intensity, while potentially a powerful tool for interpreting functionalization behavior, should not be used casually to indicate tube concentrations. Instead RBM peak shift seems to be a simpler reliable measure of functionalization behavior.

Future work is needed to corroborate our data, in particular theoretical modeling of both the RBM frequency changes and the van Hove singularity spacing modifications observed in functionalized samples. This would allow a better understanding of resonance Raman spectra of functionalized SWCNTs.

EXPERIMENTAL SECTION

Preparation of SWCNT-CO₂(CH₂CH₂O)₃CH₃ Derivatives **3a, **3b**, **3b***, and **3c**.** *Preparation of SWCNT-CO₂H Derivatives.* From Carbon Solutions and CarboLex SWCNTs **1a** and **1b**. Pristine SWCNT **1a** or **1b** (350 mg) were stirred in 53 mL of aq. nitric acid 2.6 M at 100 °C for 48 (**1a**) or 72 h (**1b**). The reaction mixture was cooled to room temperature, then the reaction medium was filtered through a polyvinylidene fluoride (PVDF) Millipore membrane (0.22 μm), and the obtained solid was washed with deionized water up to pH = 7, then with 7 mL of 0.001 M NaOH solution, this NaOH treatment being used in order to remove carboxylated carbonaceous fragments.⁴⁰ Finally the solid was washed with water (30 mL) up to neutrality, then by methanol (70 mL) to make easier the drying step. The remaining solid was dried at 110 °C under vacuum for 2 days, thus leading to ~200–230 mg purified SWCNT.

These purified SWCNT (190 mg) were added to 190 mL freshly prepared "piranha solution" (H₂SO₄ 96%/H₂O₂ 30% 4/1 v/v) previously cooled between 30 and 35 °C in an ice bath, and the resulting mixture was heated overnight at 45 °C under vigorous stirring. Then this reaction medium was transferred into an Erlenmeyer flask containing 190 g of ice. After it was cooled for 10 min, the mixture was filtered through a PVDF (0.22 μm) Millipore membrane, and washed with deionized water up to pH = 7. The remaining solid was dried overnight under vacuum giving carboxylated SWCNT-CO₂H **2a** or **2b** (~140–150 mg).

*From CarboLex and Nanoledge SWCNTs **1b** and **1c**.* Pristine SWCNT **1b** or **1c** (220 mg) were stirred in 25 mL of aq. nitric acid 2.9 M at 100 °C for 48–72 h. After it was cooled to room temperature, the reaction mixture was centrifuged 2×15 min at 1400 g. The supernate was then filtered through a PVDF (0.22 μm) Millipore membrane, then water was added to the solid residue, and the obtained suspension was again centrifuged. Both of these operations were repeated until pH = 6–7 was measured in the filtrate. The remaining solid was washed with 4 mL of 0.001 M NaOH solution and with water up to neutrality as above, and dried at 110 °C for 48 h, thus giving ~180 mg SWCNT-CO₂H derivatives **2b*** or **2c***.

Esterification of SWCNT-CO₂H Derivatives. SWCNT-CO₂H (100 mg) were stirred in 22 mL of SOCl₂ with 1 mL of dimethylformamide (DMF) at 70 °C for 24–48 h under nitrogen.³¹ After it was cooled to room temperature, the reaction mixture was centrifuged 2×15 min at 1400 g. The supernate was filtered through a polytetrafluoroethylene (PTFE 0.1 μm) Millipore membrane; dry THF was added to the obtained solid, and the resulting suspension was again centrifuged, both of these being repeated until the filtrate is colorless. The remaining solid was dried overnight under vacuum giving SWCNT-COCl (~115–120 mg).

A mixture of SWCNT-COCl (~135 mg) and alcohol HO-(CH₂CH₂O)₃-CH₃ in a large excess (4 g) was vigorously stirred at 95 °C for 96 h under nitrogen. After it was cooled to room temperature, the reaction mixture was filtered through a PTFE Millipore membrane (0.1 μm) and washed with ethanol. The remaining solid was dried under vacuum at 60 °C during one week, giving ester derivatives SWCNT-CO₂(CH₂CH₂O)₃-CH₃ **3a**, **3b**, **3b***, or **3c*** (~125–130 mg).

*Preparation of SWCNT-R Derivatives **5a**, **5c**, and **6c**.* *Preparation of Reduced SWCNT Salts.* Naphthalene (160 mg, 1.25 mmol) was dissolved, under nitrogen atmosphere, in freshly distilled and dry THF. Sodium (28 mg, 1.22 mmol) was added to this solution, then this medium was kept under stirring at room temperature, until appeared a green color, characteristic of the naphthalene anion, and sodium disappeared. This reaction medium was put in a glovebox, then added with ap-SWCNT **1a** or **1c** (148 mg, 12.3 mmol) and kept under stirring overnight at room temperature. After filtration over a PVDF membrane (0.22 μm), the remaining solid was washed with freshly distilled THF until a colorless filtrate is obtained, then dried overnight in the glovebox, thus giving crude reduced SWCNT salts **4a** or **4c**.

In a second step, crude reduced SWCNT salts (25 mg) were put into 8 g of DMSO. This mixture was stirred at room temperature for 24 h, then centrifuged under inert atmosphere for 1 h (4000 rpm or 2800 g) outside the glovebox. The tube was put again in the glovebox, two phases appearing in the tube, liquid and solid. The supernatant solution was poured into a flask, this supernatant black solution containing the soluble reduced SWCNT salts. The solid, corresponding to unreduced SWCNTs, was dried overnight and weighed, in order to determine the amount of reduced SWCNT salts dissolved in DMSO. It thus appeared that the chemical reduction of SWCNT followed the order: CarboLex << Carbon Solutions < Nanoledge, the corresponding amounts (mg) of reduced SWCNT salts dissolved in 1 g of DMSO being 0.03 << 0.2 < 1, respectively.

Functionalization of Reduced SWCNT Salts. In a glovebox, 10 equiv of halo derivative RX (C₁₂H₂₅I or BrCH₂CO₂CH₂CH₂OCH₃) are added to the reduced SWCNT salt **4a** or **4c** previously dissolved in DMSO (see above), and the reaction mixture is kept under stirring at room temperature for 48 h. Then this reaction mixture is filtered over a PTFE membrane (0.1 μm), and the remaining solid was washed successively with DMSO, ethanol, and diethyl ether, and finally dried in a desiccator under vacuum at 60 °C for 24 h, thus giving the alkylated SWCNT-C₁₂H₂₅ **5a** and **5c**, or SWCNT-CH₂CO₂CH₂CH₂OCH₃ **6c** derivatives.

Raman Spectroscopy. Carbon nanotubes were characterized by resonant Raman scattering by using several wavelengths: 561.1 nm

(diode pumped solid state laser from Cobolt), 647.1 and 676.4 nm (from a 2060 Spectra-Physics krypton ion laser) and from 700 to 750 nm with a 3900S CW Ti:Sapphire laser (pumped with an 2060 Spectra-Physics argon ion laser). In this latter case, spectra were recorded each step of 4 nm and for this reason the Rayleigh line was eliminated by using a premonochromator instead of several notch filters. Spectra were obtained on a Jobin Yvon T64000 triple subtractive spectrometer equipped with a microprobe allowing the focus of the laser spot on the sample. The laser intensity was calibrated to avoid degradation or heating of the samples. As a matter of fact, any change in the environment of the nanotubes or intertubes interactions induce shifts of the low frequency modes. This is the case when tubes initially in bundles are dispersed by using a surfactant, for which an effect similar to an hydrostatic pressure is observed.⁴¹ By illuminating the sample, its temperature can increase and therefore, the Raman mode frequencies decrease at a rate⁴² of $1\text{ cm}^{-1}/100\text{ K}$. Experimentally, spectra are recorded at RT on powders under microscope with a power limited to 1mW focused on an area of $\sim 5\text{ }\mu\text{m}$ in diameter. This represents an energy density of $\sim 5\text{ kW}/\text{cm}^2$, half of the energy density limit suggested by Olevik and all.⁴³

All spectra were obtained after an accumulation time of 2 min with a minimum resolution of 2 cm^{-1} . In the case of the systematic study performed with the Ti-sapphire laser, spectra were recorded on the same spot of a given material and corrected for the detector response in order to make intensity comparison.

Whenever curve fits had to be done, we used the Levenberg–Marquardt algorithm, based on the least-squares method. Individual bands were taken as pure Lorentzian curves.

■ ASSOCIATED CONTENT

S Supporting Information. TGA profiles issued from SWCNT-CO₂H (samples 2) and SWCNT-ester (3) derivatives, formulas used to calculate energy transitions for both semiconducting and metallic tubes, and RBM in Carbon Solutions and HIPCO samples. This material is available free of charge via the Internet at <http://pubs.acs.org>.

■ AUTHOR INFORMATION

Corresponding Author

Serge.Lefrant@cncrs-imn.fr

■ ACKNOWLEDGMENT

J.Y.M., J.P.B., C.E., and S.L. thank the ANR-2010-BLAN-0819-04 “SPRINT” for funding, and Bernard Humbert for discussions.

■ REFERENCES

- (1) Iijima, S. *Nature* **1991**, *354*, 56.
- (2) Iijima, S.; Ichihashi, T. *Nature* **1993**, *363*, 603.
- (3) Bethune, D. S.; Klang, C. H.; De Vries, M. S.; Gorman, G.; Savoy, R.; Vasquez, J.; Beyers *Nature* **1993**, *363*, 605.
- (4) Tomanek, D.; Jorio, A.; Dresselhaus, M. S.; Dresselhaus, G. *Top. Appl. Phys.* **2008**, *111*, 1.
- (5) Banerjee, S.; Hemraj-Benny, T.; Wong, S. S. *Adv. Mater.* **2005**, *17*, 17.
- (6) Herrero, M. A.; Prato, M. *Mol. Cryst. Liq. Cryst.* **2008**, *483*, 21.
- (7) Hirsch, A. *Angew. Chem., Int. Ed.* **2002**, *41*, 1853.
- (8) Dyke, C. A.; Tour, J. M. *J. Phys. Chem. A* **2004**, *108*, 11151.
- (9) Tasis, D.; Tagmatarchis, N.; Bianco, A.; Prato, M. *Chem. Rev.* **2006**, *106*, 1105.
- (10) Singh, P.; Campidelli, S.; Giordani, S.; Bonifazi, D.; Bianco, A.; Prato, M. *Chem. Soc. Rev.* **2009**, *38*, 2214.
- (11) Peng, X.; Wong, S. S. *Adv. Mater.* **2009**, *21*, 625.
- (12) Giordani, S.; Colomer, J.-F.; Cattaruzza, F.; Alfonsi, J.; Meneghetti, M.; Prato, M.; Bonifazi, D. *Carbon* **2009**, *47*, 578.
- (13) Kanungo, M.; Lu, H.; Malliaras, G. C.; Blanchet, G. B. *Science* **2009**, *323*, 234.
- (14) Bayazit, M. K.; Coleman, K. S. *J. Am. Chem. Soc.* **2009**, *131*, 10670.
- (15) Palacin, T.; Le Khanh, H.; Jousset, B.; Jegou, P.; Filoramo, A.; Ehli, C.; Guldi, D. M.; Campidelli, S. *J. Am. Chem. Soc.* **2009**, *131*, 15394.
- (16) Gebhardt, B.; Graupner, R.; Hauke, F.; Hirsch, A. *Eur. J. Org. Chem.* **2010**, 1494.
- (17) Voiry, D.; Roubeau, O.; Pénicaut, A. *J. Mater. Chem.* **2010**, *20*, 4385.
- (18) Bayazit, M. K.; Suri, A.; Coleman, K. S. *Carbon* **2010**, *48*, 3412.
- (19) Voggu, R.; Venkata Rao, K.; George, S. J.; Rao, C. N. R. *J. Am. Chem. Soc.* **2010**, *132*, 5560.
- (20) Bergeret, C.; Cousseau, J.; Fernandez, V.; Mevellec, J.-Y.; Lefrant, S. *J. Phys. Chem. C* **2008**, *112*, 16411.
- (21) Bachilo, S. M.; Strano, M. S.; Kittrell, C.; Hauge, R. H.; Smalley, R. E.; Weissman, R. B. *Science* **2002**, *298*, 2361.
- (22) Tuinstra, F.; Koenig, J. L. *J. Chem. Phys.* **1970**, *53*, 1126.
- (23) Thomsen, C.; Reich, S. *Phys. Rev. Lett.* **2000**, *85*, 5214.
- (24) Abdula, D.; Nguyen, K. T.; Shim, M. *J. Phys. Chem. C* **2007**, *111*, 17755.
- (25) Rochefort, A.; Avouris, P. *J. Phys. Chem. A* **2000**, *104*, 9807.
- (26) Liu, J.; Dossot, M.; Olevik, D.; Mamane, V.; Vigolo, B.; Abrahamsson, D.; Jonsson, H.; Fort, Y.; Humbert, B.; Soldatov, A. V.; McRae, E. *Phys. E* **2008**, *40*, 2343.
- (27) Pénicaut, A.; Poulin, P.; Derré, A.; Anglaret, E.; Petit, P. *J. Am. Chem. Soc.* **2005**, *127*, 8.
- (28) Voiry, D.; Roubeau, O.; Pénicaut, A. *J. Mater. Chem.* **2010**, *20*, 4385.
- (29) Liu, J.; Rinzler, A. G.; Dai, H.; Hafner, J. H.; Bradley, R. K.; Boul, P. J.; Lu, A.; Iverson, T.; Shelimov, K.; Huffman, C. B.; Rodriguez-Macias, F.; Shon, Y.-S.; Lee, T. R.; Colbert, D. T.; Smalley, R. E. *Science* **1998**, *280*, 1253.
- (30) Ziegler, K. J.; Gu, Z.; Peng, H.; Flor, E. L.; Hauge, R. H.; Smalley, R. E. *J. Am. Chem. Soc.* **2005**, *127*, 1541.
- (31) Bonifazi, D.; Nacci, C.; Marega, R.; Campidelli, S.; Ceballos, G.; Modesti, S.; Meneghetti, M.; Prato, M. *Nano Lett.* **2006**, *6*, 1408.
- (32) Andersson, C.-H.; Grennberg, H. *Eur. J. Org. Chem.* **2009**, 4421.
- (33) Figueiredo, J. L.; Pereira, M. F. R.; Freitas, M. M. A.; Orfao, J. J. M. *Carbon* **1999**, *37*, 1379.
- (34) Tchoul, M. N.; Ford, W. T.; Lolli, G.; Resasco, D. E.; Arepalli, S. *Chem. Mater.* **2007**, *19*, 5765.
- (35) Kataura, H.; Kumazawa, Y.; Maniwa, Y.; Umczu, I.; Suzuki, S.; Ohtsuka, Y.; Achiba, Y. *Synth. Met.* **1999**, *103*, 2555.
- (36) Maultzsch, J.; Pomraenke, R.; Reich, S.; Chang, E.; Prezzi, D.; Ruini, A.; Molinari, E.; Strano, M. S.; Thomsen, C.; Lienau, C. *Phys. Rev. B* **2005**, *72*, 241402.
- (37) See, for example: Dresselhaus, M. S.; Dresselhaus, G.; Jorio, A.; Souza Filho, A. G.; Saito, R. *Carbon* **2002**, *40*, 2043.
- (38) Meyer, J. C.; Paillet, M.; Michel, T.; Moréac, A.; Neumann, A.; Duesberg, G.; Roth, S.; Sauvajol, J. L. *Phys. Rev. Lett.* **2005**, *95*, 217401.
- (39) Müller, M.; Meinke, R.; Maultzsch, J.; Syrgiannis, Z.; Hauke, F.; Pekker, A.; Kamaras, K.; Hirsch, A.; Thomsen, C. *ChemPhysChem* **2010**, *11*, 2444.
- (40) Salzmann, C. G.; Ijwellyn, S. A.; Tobias, G.; Ward, M. A. H.; Huh, Y.; Green, M. L. H. *Adv. Mater.* **2007**, *19*, 883.
- (41) Izard, N.; Riehl, D.; Anglaret, E. *Phys. Rev. B* **2005**, *71*, 195417.
- (42) Li, H. D.; Yue, K. T.; Lian, Z. L.; Zhan, Y.; Zhou, L. X.; Zhang, S. L.; Shi, Z. J.; Gu, Z. N.; Liu, B. B.; Yang, R. S.; Yang, H. B.; Zou, G. T.; Zhang, Y.; Iijima, S. *Appl. Phys. Lett.* **2000**, *76*, 2053.
- (43) Olevik, D.; Soldatov, A. V.; Dossot, M.; Vigolo, B.; Humbert, B.; McRae, E. *Phys. Status Solidi B* **2008**, *245* (10), 2212.